Proceedings of the ASME 2021
International Mechanical Engineering Congress and Exposition
IMECE2021
November 1-5, 2021, Virtual, Online

IMECE2021-68680

FRESH AIR FLOW REQUIRED TO MAINTAIN SAFE CARBON DIOXIDE LEVELS AND PROVIDE A BREATHABLE AIR ENVIRONMENT IN A REFUGE ALTERNATIVE

Cory DeGennaro[1], Lincan Yan, David Yantek
CDC/NIOSH
Pittsburgh, PA, USA

ABSTRACT

Federal mining regulations in the United States mandate that underground coal mines install refuge alternatives (RA) for miners to seek refuge after an inescapable disaster. RAs are required to isolate and protect occupants from hazardous conditions and to provide a life-sustaining, breathable air environment for a minimum of 96 hours. According to federal RA regulations, an RA's oxygen levels (%O_2) must be maintained between 18.5%–23% with carbon dioxide levels (%CO_2) less than 1%. Once an RA is occupied, due to human breathing, the %O_2 can decrease, and %CO_2 levels can increase quickly. One method of providing an RA with a breathable air environment is to use a borehole air supply (BAS) to provide fresh air from the surface, purge existing harmful gases, and prevent harmful gas build-up. RA regulations require air supplies to provide air at 12.5 cubic feet per minute (cfm) per person. To investigate the minimum fresh air flow (FAF) rate needed to maintain interior %O_2 and %CO_2 within the mandated ranges, researchers conducted testing in a modified shipping container that represented the volume of an RA. During these tests, propane (C_3H_8) combustion and additional CO_2 supplied from cylinders were used to match human O_2 consumption and CO_2 generation. The FAF rate supplied to the shipping container was varied to determine the minimum FAF rate required for the %CO_2 inside the shipping container to stabilize below 1%. The test results showed that the minimum FAF rate was between 1.76–2.12 cfm per person. Therefore, the mandated per-person FAF rate provides a 6x–7x safety factor. Test results also showed that the %O_2 range requirement was satisfied for the entire range of tested FAF rates from 1.76–12.5 cfm per person.

In this paper, researchers from the National Institute for Occupational Safety and Health (NIOSH) provide a repeatable test method that can be used to evaluate the FAF rate versus interior gas concentrations (%CO_2 and %O_2) for various occupancy levels to ensure a breathable air environment within a refuge alternative. This paper also discusses federal RA regulations and previous NIOSH research. Additionally, this paper provides an experimental concept and set-up description, including the C_3H_8 combustion and supplemental CO_2 delivery with gas flow rates used to simulate human breathing, data collection sensors, laboratory modifications, and safety measures. Lastly, the paper discusses test results, including the amount of time taken to reach hazardous interior %CO_2 and %O_2, as well as %O_2 and %CO_2 resulting from several FAF rates that have been used to validate a predictive model. This test method could be adopted to evaluate breathable air environments in refuge alternatives and confined enclosures in various industries.

Keywords: Refuge alternatives, carbon dioxide, breathable air, confined space

NOMENCLATURE

%CO_2	carbon dioxide concentration
%O_2	oxygen concentration
BAS	borehole air supply
BIP RA	built-in-place refuge alternative
C_3H_8	propane
CO_2	carbon dioxide
cfh	cubic feet per hour
cfm	cubic feet per minute
FAF	fresh air flow
HBS	human breathing simulator
NIOSH	National Institute for Occupational Safety and Health
O_2	oxygen
ppm	parts per million
PRVTS	pressure relief valve test stand
RA	refuge alternative

[1] Corresponding author. Cdegennaro@cdc.gov

1. INTRODUCTION

Federal regulations mandate underground coal mines in the United States to position refuge alternatives (RA) 1,000 feet from the working face and 30 minutes travel distance (walking) outby for miners to seek refuge following a disaster where escape is not possible. RAs must be designed to provide a life-sustaining environment for a minimum of 96 hours by meeting several criteria for approval [1]. One of the most crucial functions of an RA is providing a breathable air environment, which is partially defined as one with 18.5%–23% oxygen levels (%O_2) and carbon dioxide levels (%CO_2) below 1% with excursions not to exceed 2.5% [1].

RA regulations also include a space requirement of 15 square feet per person and a volume requirement of 30–60 cubic feet per person based on mine height [1]. For example, a mine height of 54 inches or greater corresponds to 60 cubic feet per person. These requirements limit the allowable number of occupants within an RA. RA manufacturers must take this into account during the design phase. Likewise, mine operators must also consider this as well as the number of miners, contractors, and visitors that may be present in a working area at any given time when determining the appropriate size and type of RA for certain areas.

Three types of RAs are approved for use in underground U.S. coal mines including portable and built-in-place (BIP RA) variations [2]. The portable classification includes two types: rigid steel and tent-type. Portable RAs provide a breathable air environment via O_2 cylinders. Federal regulations state that these RAs must provide O_2 at a rate of 1.32 cfh per person via the O_2 cylinders [1]. A BIP RA is essentially a mined-out area with a stopping and man-door installed to create a permanent room. To create a breathable air environment, BIP RAs can also use O_2 cylinders at the previously mentioned flow rate or a borehole air supply (BAS) with a fan or compressor located on the surface to provide breathable air at a rate of 12.5 cfm per person [1]. Since hazardous gas levels may exist within the RA after entry, adequate controls must be implemented to limit an additional build-up of gases produced by occupants.

Existing standards and previous research studies on the relationship between ventilation and %CO_2 as well as health effects of %CO_2 and %O_2 were reviewed. CO_2 exposure can produce adverse health effects, such as respiratory symptoms and decreased cognitive performance, at concentrations ranging between 1,000 ppm–10,000 ppm and as low as 500 ppm in some cases [3–9]. The ASHRAE ventilation standard 62.1 states that a ventilation rate of 15 cfm per person will limit the %CO_2 to 1,000 ppm [10]. Two studies citing this standard state that complaints have been reported of poor air quality for concentrations between 700–800 ppm [11, 12]. Additionally, the Occupational Safety and Health Administration (OSHA) considers an atmosphere consisting of less than 19.5% O_2 to be O_2 deficient and immediately dangerous to life or health (IDLH) and recognizes that negative health effects can occur in some workers performing work-related tasks [13, 14]. Other research shows that adverse health effects resulting from exposure to O_2 deficient environments do not occur until the %O_2 falls to 16% or below [15, 16]. However, federal RA regulations aim to prevent the RA atmosphere from reaching these low concentrations by preventing the build-up of and removing harmful gases from the RA as well as providing sufficient breathable air to maintain a minimum of 18.5% O_2.

A critical RA regulation component examined in this study is the minimum amount of fresh air necessary to prevent the build-up of CO_2 while providing enough breathable air. As previously mentioned, %CO_2 must be maintained at 1% or less with excursions no greater than 2.5%. For RAs that use O_2 cylinders to provide a breathable air environment, CO_2 scrubbers are needed because O_2 is not provided at a high enough rate to yield sufficient air exchange to prevent CO_2 build-up. These RAs use CO_2 scrubbing systems, which are available as soda lime or lithium hydroxide cartridges or curtains that remove the CO_2 from the environment through a chemical reaction which generates heat and moisture. RA CO_2 scrubbing systems must be designed to remove 1.08 cfm per person of CO_2 [1]. Generally, RAs that implement a BAS do not require CO_2 scrubbing systems as the higher fresh air flow (FAF) rate provides enough air exchanges to prevent CO_2 build-up. However, the relationship between the FAF rate and occupied RA %CO_2 is unknown. Therefore, NIOSH researchers investigated the relationship between the FAF rate and occupied RA %CO_2 to determine the possible safety factor provided by the 12.5 cfm per person FAF requirement. This was accomplished by simulating human O_2 consumption and CO_2 generation for a desired number of occupants while providing a range of FAF rates to the enclosure and monitoring the interior conditions.

2. EXPERIMENTAL SET-UP AND METHOD

2.1. Concept and overview

The first matter that was addressed was the human O_2 consumption and CO_2 generation simulation approach. Researchers determined that C_3H_8 (propane) combustion was a feasible method to consistently consume O_2 and generate CO_2 at predictable rates. Another component of the experimental concept was identifying a FAF delivery source. A pressure relief valve test stand (PRVTS), developed by NIOSH for previous RA-related research on relief valves, was repurposed to provide controllable FAF because it incorporates a variable frequency drive to adjust the speed of a centrifugal fan, which in turn adjusts the FAF rate [17]. In addition, the PRVTS uses an air flow measurement station to measure the volume flow rate of air provided. Researchers determined that a shipping-container-based laboratory reasonably mimics an RA. O_2 and CO_2 sensors were installed inside the laboratory to monitor %CO_2 and %O_2 for data collection purposes.

2.2. C_3H_8 (propane) combustion

C_3H_8 combustion is a well-known chemical process that can be easily controlled by adjusting the C_3H_8 and combustion air flow rates. The combustion process consumes C_3H_8 and O_2 and generates CO_2 and water. The O_2 needed for combustion is supplied in the form of atmospheric air which has an average

composition of 79% nitrogen and 21% O_2. Therefore, researchers used the C_3H_8 combustion reaction equation (Eqn. 1) to calculate the flow rates that were required to maintain complete combustion [18].

$$C_3H_8 + 5O_2 = 3CO_2 + 4H_2O \quad (1)$$

Eqn. 1 was applied to C_3H_8 combustion using mass flow controllers to set the rates of C_3H_8 and combustion air. All mass flow rates were established on a per-person basis to allow scaling for a desired number of represented occupants. The known input used in Eqn. 1 was the per-person O_2 consumption of 1.32 cfh or 0.80 grams/minute specified by the RA regulation. By setting the per person O_2 consumption and the number of represented occupants, researchers calculated the mass flow rates of C_3H_8 and combustion air needed. Approximately 20% excess combustion air was used to ensure complete combustion. The mass flow rate of CO_2 generated by combustion was also calculated as 0.66 grams/minute using Eqn. 1. The mass flow rate of CO_2 generated by human breathing was estimated using the CO_2 removal rate specified in the RA regulation: 1.08 cfh or 0.90 grams/minute per person. Since C_3H_8 combustion generates less CO_2 than human breathing, supplemental CO_2 was required to match the CO_2 removal rate. Table 1 shows all gas mass flow rates used during testing on a per-person basis.

Table 1: Mass flow rates for C_3H_8 combustion and supplemental CO_2.

Type of gas	Approximate mass flow rate per person (grams/minute)
O_2 to be consumed	0.80
C_3H_8 needed to consume O_2	0.22
Combustion air (including 20% excess)	4.45
CO_2 from combustion	0.66
CO_2 from human breathing	0.90
Supplemental CO_2 needed (Human breathing - Combustion)	0.24

2.3. Human Breathing Simulator (HBS)

Rather than designing and developing a novel C_3H_8 combustion device, researchers used a commercially available Dyna-Glo C_3H_8 gas smoker with two burners to burn C_3H_8 and act as a human breathing simulator (HBS). This is an ideal apparatus for testing since burning C_3H_8 is its intended purpose, and it has a simple, compact, and easily modified design.

Controlling the combustion process was crucial to ensure consistent burning throughout testing. To ensure that all combustion air delivered to the smoker was measurable, a sealed combustion chamber was created by sealing all gaps and openings beneath the burners and between the smoker's legs. An Alita AL-400 air pump was located inside the laboratory and plumbed into the closed space below the burners via a flared duct to minimize the inlet velocity and turbulence to maintain a stable flame. Locating the air pump within the laboratory ensures the burners are provided combustion air from inside the laboratory in a similar manner as RA occupants in a real-life scenario. An Alicat Scientific MCR-250SLPM mass flow controller was installed outside of the laboratory in line with the air pump to allow access for combustion air mass flow rate adjustments during testing without entering the laboratory. Likewise, an Alicat Scientific MC-10SLPM mass flow controller was installed in line between the C_3H_8 burner and C_3H_8 cylinders to precisely control the amount of C_3H_8 delivered to the combustion chamber.

Continuous and clean combustion was an essential component of the HBS to ensure the recorded data represented human O_2 consumption. Incomplete combustion could generate carbon monoxide which would negatively affect test results and could compromise safety within the laboratory and test area [18]. Aluminum HVAC ductwork was mounted on top of the smoker, and a Michell XZR200 Oxygen Analyzer, an Edinburgh Sensors Guardian NG, and a Bacharach Fyrite InTech Efficiency Analyzer were installed to measure the $\%O_2$, $\%CO_2$, and flue or combustion gases, respectively. The combustion gas analyzer was most significant because it indicated any carbon monoxide generation. These data verified clean combustion as a safety check and were not recorded.

As stated above, for a specified O_2 consumption rate, the CO_2 generation rate from C_3H_8 combustion is less than the generation rate from human breathing. Therefore, a simple CO_2 delivery system consisting of a CO_2 cylinder, regulator, and a Cole Parmer 10 L/min Masterflex mass flow controller was incorporated into the HBS to add supplemental CO_2 to match the CO_2 generated by people for a given O_2 consumption rate. The mass flow controller was installed on the outside of the laboratory like the others allowing researchers to adjust the gas flow rate during testing without entering the laboratory.

Additional safety measures were taken to ensure the flame remained stable throughout testing. Researchers modified the smoker and installed two sight windows near the flame. The first was for a video camera to monitor the flame which should remain a blue shade and relatively steady. A Rel-tek Spot Fire flame detector that monitored the presence of a flame was installed at the second window and served two purposes. If the flame went out, C_3H_8 would continue flowing into the smoker and create a potentially explosive environment. Therefore, the flame detector's main function was to shut off C_3H_8 flow via a solenoid valve installed on the C_3H_8 delivery line if no flame was detected. The secondary function of the detector was to notify researchers if there was no flame using an audible strobe alarm.

2.4. Laboratory and sensors

Researchers modified a standard 8' x 8' x 20' steel shipping container into a test laboratory. The laboratory's floor area was 160 square feet with a total volume of 1,280 cubic feet. An enclosure of this size satisfies the RA volume requirements for 21 people. Ventilation ductwork with check valves on the inlet and outlet was installed on the laboratory to provide fresh

air to the interior using the PRVTS. A man-door was installed on one side of the shipping container as an access location. Once all modifications to the laboratory were complete and all equipment was installed, the double doors on the end of the shipping container were closed and sealed using expanding foam. Also, all penetrations created to install any gas fittings, data cables, or power lines on the laboratory were sealed using duct seal compound. Additional gaps on the man-door were sealed using duct seal compound and aluminum tape during testing to minimize loss out of the laboratory and to maintain positive pressure.

Various data-related sensors were installed inside the laboratory to measure interior conditions. Three Macurco OX-6 O_2 sensors and two CTI GG-CO2 CO_2 sensors were installed to monitor the interior $\%O_2$ and $\%CO_2$. The O_2 sensors have a range of 0%–25% by volume. The CO_2 sensors have a range of 0%–5% by volume. Two of the O_2 sensors and the CO_2 sensors were located approximately 6.5 feet and 13 feet from the end of the laboratory. The third O_2 sensor was positioned near the HBS air pump to verify the $\%O_2$ in the combustion air.

Aside from the O_2 and CO_2 sensors to measure the interior $\%CO_2$ and $\%O_2$, additional gas detectors were used to ensure safety during testing. Researchers used a Bacharach Leakator 10 combustible gas leak detector to perform a safety check before each test. An RKI Instruments Beacon 800 gas monitoring system with several sensors was installed as the key safety system to monitor the interior $\%O_2$, carbon monoxide, and $\%CO_2$, as well as the C_3H_8 lower explosive limit (%LEL). The %LEL sensor was installed near the connection point between the C_3H_8 line and smoker. Two previously mentioned safety measures were used to monitor for a stable flame during testing—the video monitoring system and the Rel-tek flame detector. Vaisala HMP-110 temperature and relative humidity sensors were also installed inside the laboratory as a safety measure to ensure a safe temperature.

2.5. PRVTS

A pressure relief valve test stand (PRVTS) was chosen as the FAF delivery source [17]. The PRVTS consists of a centrifugal fan, variable frequency drive (VFD), and a VELTRON air flow measurement station. Adjusting the VFD allows for an air flow range of 100–1,100 cfm. The VELTRON measures the air flow in cfm or FAF rate. The PRVTS was positioned outside of the laboratory and connected to the existing laboratory ventilation inlet via insulated, flexible ductwork. In a mining application, this PRVTS is mimicking a BAS that would provide the breathable air to occupants within the RA.

2.6. Data collection equipment

A Data Translation DT9874 MEASURpoint data acquisition system was used to measure gas concentrations, temperature, relative humidity, FAF rate, and gas mass flow rates. All data were recorded at a sample rate of 0.5 samples per second with 24-bit resolution. A higher sample rate was unnecessary because the data did not change quickly. To reduce noise in the measurements, a software-selectable 16-point moving average was applied to all measured data. An application named QuickDAQ was used to log and visualize the real-time data which allowed researchers to ensure safe conditions were maintained and to determine if adjustments were required. Microsoft Excel was used for post-processing and data plotting.

2.7. Procedure

Prior to beginning a test, the data recording was started, and researchers used the Bacharach Leakator to check for leaks along the gas line and for C_3H_8 accumulation within the smoker. Once a safe gas line and smoker status was confirmed, the C_3H_8 flow was started, and the burners were ignited. Next, supplemental CO_2 was introduced into the laboratory once a steady flame was achieved. Then, the man-door was sealed, and testing began by initiating the PRVTS at the specified FAF rate of 12.5 cfm per person. Each mass flow controller was set to the flow rate needed to represent the number of occupants using the values from Table 1. Researchers allowed the test to continue for up to two hours for each FAF rate or until the interior $\%CO_2$ stabilized. If the $\%CO_2$ stabilized below 1%, the FAF rate was reduced by 50%. If the $\%CO_2$ stabilized or increased above 1%, the FAF rate was increased by 50% of the difference between the current and previous FAF rates. This iterative method using integer multiples or divisions of the regulated FAF rate was implemented to identify the relationship between FAF rate and $\%CO_2$.

3. RESULTS AND DISCUSSION

Researchers conducted tests to investigate the relationship between the FAF rate delivered to an enclosed space and the resulting interior $\%CO_2$ averaged between the two sensor locations. The first test represented 21 occupants with the PRVTS delivering FAF at a rate of 12.5 cfm per person. The $\%CO_2$ stabilized at 0.2% after around 70 minutes, so researchers reduced the FAF rate by 50% to 6.25 cfm per person. Eighty minutes after reducing the FAF rate, the $\%CO_2$ then stabilized at 0.37%. Once this test concluded, researchers determined that the FAF rate needed to be reduced below the VELTRON measurable range to allow the $\%CO_2$ to increase and stabilize at 1%. Therefore, to ensure the minimum FAF rate was greater than the lower measurable range of the airflow meter, 100 cfm, the number of represented occupants was increased by increasing the mass flow rates for each gas according to Table 1. As a result, researchers conducted tests that represented 21, 34, 40, 48, and 58 occupants with the same minimum FAF rate limitation until 58 occupants were represented.

All tests exhibited an increase in $\%CO_2$ with time following a FAF rate reduction. For example, Figure 1 shows the 40-occupant test with multiple FAF rates per person (12.5, 6.25, 4.13, 3.1, 2.55 cfm) and the resulting $\%CO_2$. Figure 1 also illustrates the need to increase the number of represented occupants because the $\%CO_2$ did not reach 1% when 102 cfm (2.55 cfm x 40 occupants) was used since it was near the minimum measurable FAF rate. Figure 2 displays that the

resulting $\%O_2$ remained in the mandated range for the same FAF rates per person mentioned above.

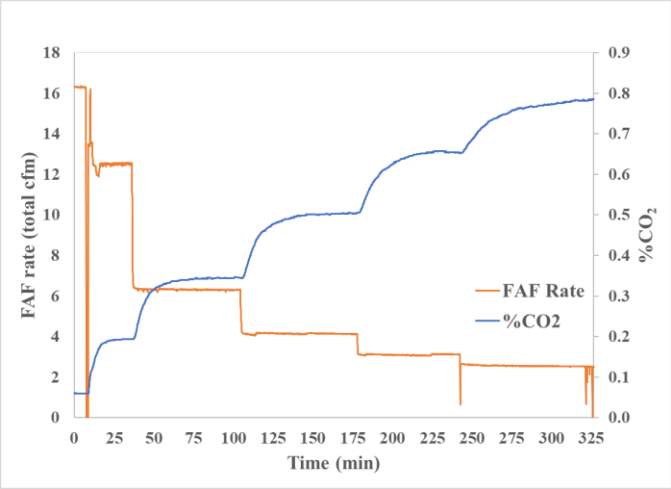

Figure 1: Resulting $\%CO_2$ increases for various FAF rate reductions during 40-occupant test.

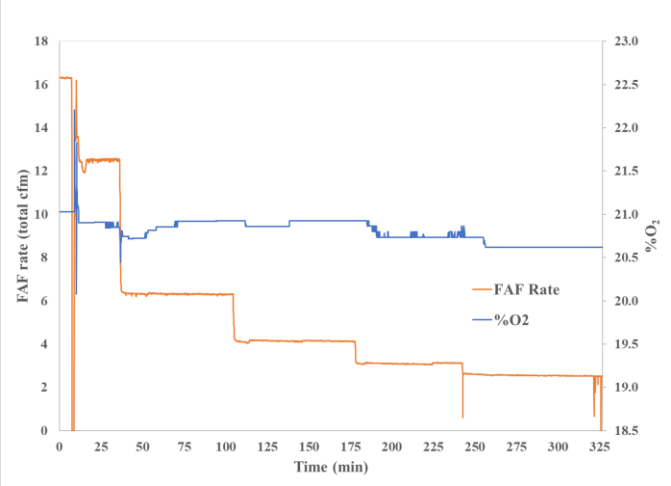

Figure 2: Resulting $\%O_2$ for various FAF rate reductions during 40-occupant test.

Table 2 displays the results for each test including the number of represented occupants, FAF rates used, and the resulting average $\%CO_2$. The time column in Table 2 indicates the amount of time researchers allowed for each FAF rate. Some tests reached steady state, while others were cut short as researchers determined that the interior $\%CO_2$ would not reach 1% resulting in single-FAF test durations ranging between 18–115 minutes. Table 2 also includes the safety factor that the mandated FAF rate would provide compared to the FAF rates used during testing.

Table 2: Summary of FAF rate versus $\%CO_2$ test results for various numbers of represented occupants.

# Occupants	Total FAF Rate (cfm)	FAF rate per Occupant (cfm)	Time* (min)	% CO_2
21	262.5	12.5	100	0.2
	131	6.2	100	0.37
34	425	12.5	18	0.18
	102	3	21	0.54
40	500	12.5	30	0.19
	250	6.25	67	0.34
	165	4.13	72	0.50
	124	3.1	65	0.65
	102	2.55	70	0.79
48	600	12.5	75	0.2
	121	2.52	90	0.78
	103	2.15	75	0.9
58	102	1.76	115	1.1
	123	2.12	31	0.93

As expected, the interior $\%O_2$ remained within the RA regulation range of 18.5%–23% for all tests. As shown in Table 2, the $\%CO_2$ did not reach 1% until the FAF per person was 1.76 cfm, which was achieved during the 58-occupant tests. Researchers then increased the FAF rate to 2.12 cfm per person, which reduced the $\%CO_2$ to around 0.93%. Assuming a constant relationship within this range, the FAF rate corresponding to 1% CO_2 would fall between 1.76–2.12 cfm per person, as shown in Figure 3. Therefore, the safety factor range provided by the RA regulations would be approximately 6x–7x. Although these lower FAF rates may be sufficient, the mandated FAF rate provides additional safety for occupants by diluting contaminants faster to achieve a breathable air environment. Additionally, Figure 4 shows the resulting $\%O_2$ for the FAF rates per person used during the 58-occupant test.

* These are the elapsed times for each FAF rate as some tests were ended prior to reaching steady state.

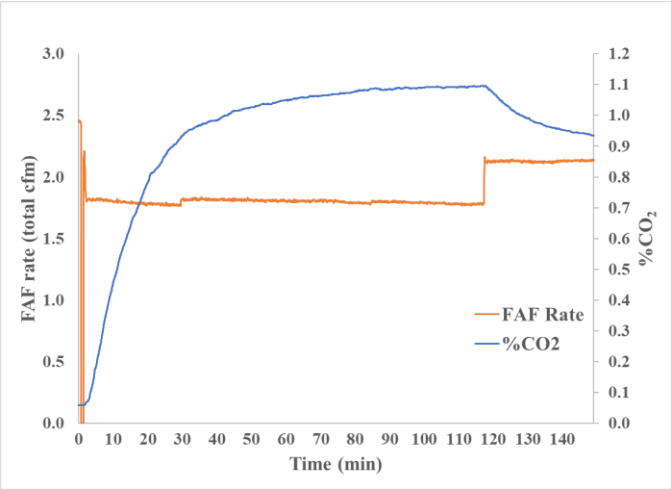

Figure 3: Resulting $\%CO_2$ of 1.1% (FAF rate of 1.76 cfm per person) and 0.93% (FAF rate of 2.12 cfm per person).

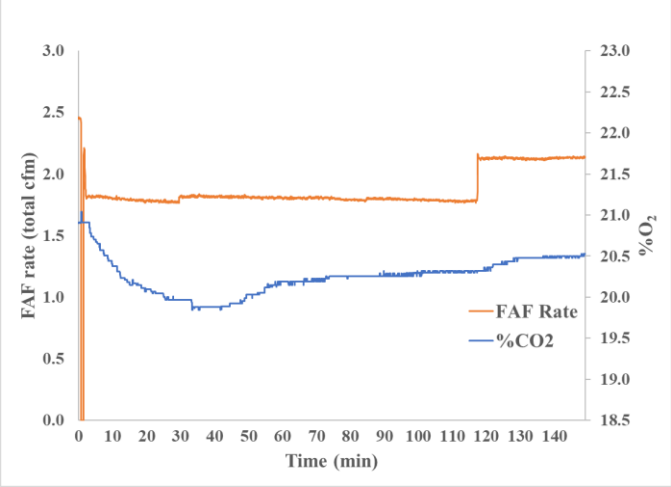

Figure 4: Resulting $\%O_2$ for FAF rates of 1.76 and 2.12 cfm per person.

A predictive, mathematical model representing this relationship was developed and validated using the test data above [19]. The model accounts for the enclosure's volume, initial $\%CO_2$, occupant CO_2 generation rate, and FAF rate. The model predicted that the interior $\%CO_2$ would stabilize at 1% if the FAF rate was ~1.87 cfm per person, implying a safety factor of 6.7x, which falls into the test data range.

Tests with zero FAF delivered to the laboratory and no CO_2 removal method were also conducted to demonstrate how quickly the interior would reach hazardous $\%CO_2$ and $\%O_2$ levels and to provide more data for the predictive model [19]. Like the previous tests, the HBS and supplemental CO_2 were used to simulate O_2 consumption and CO_2 generation. Figures 5–6 present the decrease in O_2 and increase in CO_2 with no FAF delivery system in place. As shown in Figure 5, the $\%O_2$ decreased below 18.5% within 65 minutes and nearly reached 18% within 75 minutes. Likewise, Figure 6 shows the $\%CO_2$ surpassed 1% within 40 minutes and 2% within 75 minutes. The plots indicate that this trend would continue until the O_2 within the laboratory was consumed, which would terminate the combustion process due to lack of O_2. Additionally, the $\%CO_2$ would continue to rise to dangerous levels. These two factors confirm the importance of promptly supplying enough breathable air and decreasing the $\%CO_2$.

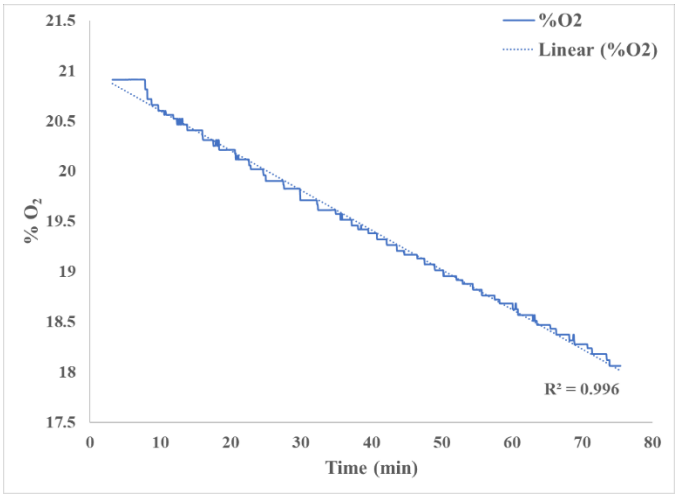

Figure 5: $\%O_2$ decreased below 18.5% while representing 21 occupants with zero FAF delivered.

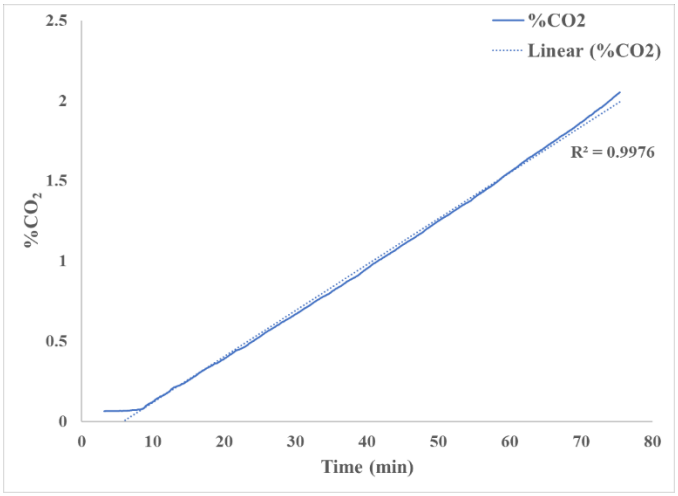

Figure 6: $\%CO_2$ increased above 2% while representing 21 occupants with zero FAF delivered.

4. CONCLUSION

The objective of this study was to identify the relationship between the required FAF rate per person to maintain an interior O_2 range of 18.5%–23% with a maximum of 1% CO_2 within an enclosed space or RA. A C_3H_8 combustion-based human breathing simulator and supplemental CO_2 was implemented to consume O_2 and generate CO_2 at the rate of a human. For tests with FAF delivery, researchers represented occupants within an enclosure and identified that a FAF rate range of 1.76–2.12 cfm per person is required to provide enough breathable air and mitigate the CO_2 increase to 1%. This indicates that the mandated FAF rate of 12.5 cfm per person provides a safety factor of 6x–7x compared to the test results. For tests with zero FAF delivery, test results show that the mandated ranges of 1%

CO_2 and 18.5% O_2 were reached within 40 minutes and 65 minutes, respectively.

The limitations of this study include testing only one simulated RA volume with one air delivery configuration. However, similar results would be expected for other RA volumes. This test method and procedure could be used to evaluate breathable air environments in RAs of different volumes as well as enclosures in various industries.

ACKNOWLEDGEMENTS

The authors wish to thank Brandin Lambie, Jeff Yonkey, Justin Srednicki, Pat McElhinney, John Homer, and Rohan Fernando of NIOSH for their support in designing the experiment, modifying the test laboratory, installing instrumentation, and conducting the experiment. The authors also wish to thank representatives of the Mine Safety and Health Administration, Approval and Certification Center, Applied Engineering Division for their feedback throughout the experiment design and execution phases.

DISCLAIMER

The findings and conclusions in this paper are those of the authors and do not necessarily represent the official position of the National Institute for Occupational Safety and Health, Centers for Disease Control and Prevention. Mention of any company or product does not constitute endorsement by NIOSH.

REFERENCES

[1] Code of Federal Regulations, Title 30 CFR, Mineral Resources, Mine Safety and Health Administration (MSHA), U.S. Department of Labor, December 31, 2008, MSHA.GOV, 30 CFR Parts 7 Subpart L (Refuge Alternatives) and 75 Subpart P (MINE EMERGENCIES)

[2] NIOSH, 2015, "Facilitating the use of built-in-place refuge alternatives in mines." By Trackemas, J.D., Thimons, E.D., Bauer, E.R., Sapko, M.J., Zipf, R.K., Schall, J., Rubinstein, E., Finfinger, G.L., Patts, L.D., LaBranche, N., Pittsburgh, PA: U.S. Department of Health and Human Services, Centers for Disease Control and Prevention, National Institute for Occupational Safety and Health, DHHS (NIOSH) Publication No. 2015-114, RI 9698.

[3] DHEW, 1976, Rockville, MD: U.S. Department of Health, Education, and Welfare, Public Health Service, Centers for Disease Control, National Institute for Occupational Safety and Health, DHEW (NIOSH) Publication No. 76-194, 1976 Aug; Pp. 1-180. https://www.cdc.gov/niosh/docs/76-194/

[4] Jung, S. H., Grady, M. L., Victoroff, T., Miller, A. L., 2017. "Simultaneously Reducing CO2 and Particulate Exposures via Fractional Recirculation of Vehicle Cabin Air." Atmospheric Environment. Volume 160 pp 77–88. ISSN 1352-2310. http://dx.doi.org/10.1016/j.atmosenv.2017.04.014

[5] Zhang, J., Pang, L., Cao, X., Wanyan, X., Wang, X., Liang, J., Zhang, L., 2020. "The Effects of Elevated Carbon Dioxide Concentration and Mental Workload on Task Performance in an Enclosed Environmental Chamber." Building and Environment. Volume 178. ISSN 0360-1323. https://doi.org/10.1016/j.buildenv.2020.106938

[6] Allen, J. G., MacNaughton, P., Satish, U., Santanam, S., Vallarino, J., Spengler, J. D., 2016. "Associations of Cognitive Function Scores with Carbon Dioxide, Ventilation, and Volatile Compound Exposures in Office Workers: A Controlled Exposure Study of Green and Conventional Office Environments." Environmental Health Perspectives. Volume 124. No. 6. June 2016. Pp. 805–812. http://dx.doi.org/10.1289/ehp.1510037

[7] Hudda, N., Fruin, S. A., 2017. "Carbon dioxide accumulation inside vehicles: The effect of ventilation and driving conditions." Science of the Total Environment. Volumes 610–611. 2018. ISSN 0048-9697. Pp 1448–1456. http://dx.doi.org/10.1016/j.scitotenv.2017.08.105

[8] Azuma, K., Kagi, N., Yanagi, U., Osawa, H., 2018. "Effects of low-level inhalation exposure to carbon dioxide in indoor environments: A short review on human health and psychomotor performance." Environmental International. Volume 121. Pp. 51–56. https://doi.org/10.1016/j.envint.2018.08.059

[9] Zhang X., Wargocki P., Lian Z., Thyregod C., 2017. Effects of exposure to carbon dioxide and bioeffluents on perceived air quality, self-assessed acute health symptoms, and cognitive performance. Indoor Air. 2017 Jan;27(1):47-64. doi: 10.1111/ina.12284. Epub 2016 Mar 7. PMID: 26825447.

[10] "Minimum Ventilation Rates in Breathing Zone," ASHRAE 62.1-2019, Ventilation for Acceptable Indoor Air Quality, American Society of Heating, Refrigeration, and Air-Conditioning Engineers, 2019, pp. 17–20, ISSN 1041-2336, Standard 62.1-2019 - American Society of Heating, Refrigerating and Air-Conditioning Engineers (iwrapper.com).

[11] Alberts, W. M., 1994. "Indoor air pollution: NO, NO2, CO, and CO2." J Allergy Clin. Immunol. Volume 94, Number 2, Part 2. Pp. 289-295. ISSN 0091-6749. https://doi.org/10.1053/ai.1994.v94.a56007

[12] WSUEEP, 2000. "Why Measure Carbon Dioxide Inside Buildings?" By Prill, R., Washington State University Extension Energy Program, WSUEEP07-003, Microsoft Word - CO2 in Buildings.doc (wsu.edu).

[13] Code of Federal Regulations, Title 29 CFR, Labor, Occupational Safety and Health Administration, Department of Labor, April 20, 2006, 29 CFR Part 1910, Subpart I, Standard Number 1910.134. 1910.134 - Respiratory Protection. | Occupational Safety and Health Administration (osha.gov)

[14] Code of Federal Regulations, Title 29 CFR Standard Interpretations, Occupational Safety and Health Administration, Department of Labor, April 2, 2007, "Clarification of OSHA's requirement for breathing air to have at least 19.5 percent oxygen content." https://www.osha.gov/laws-regs/standardinterpretations/2007-04-02-0#:~:text=Breathing%20air%20containing%206%20to,These%20symptoms%20occur%20immediately.

[15] NWOHS, 2009. "Oxygen: Health Effects and Regulatory Limits Part I: Physiological and Toxicological Effects of Oxygen Deficiency and Enrichment." By McManus, N., NorthWest Occupational Health and Safety, "Excerpts from Safety and Health in Confined Spaces," https://www.remtech.no/wp-content/uploads/2017/11/Oxygen-Regulatory-Limits-I.pdf.

[16] NIOSH, 1987. "A Guide to Safety in Confined Spaces." By Pettit, T., Linn, H., U.S. Department of Health and Human Services, Centers for Disease Control and Prevention, National Institute for Occupational Safety and Health, DHHS (NIOSH) Publication No. 87-113. A Guide to Safety in Confined Spaces (87-113) | NIOSH | CDC.

[17] Lutz T.J., Yonkey J.A., 2018. "Refuge alternatives relief valve testing and design with updated test stand." Min Eng, 70(3):46-50.

[18] Hahn, Eric. "Incomplete & Complete Combustion of Propane – Propane Equation and Formula." ELGAS LPG Gas Blog, November 9, 2019. https://www.elgas.com.au/blog/2208-complete-incomplete-combustion-of-lpg-propane-equations.

[19] Yan, L., Yantek, D. S., DeGennaro, C. R., Fernando, R. D., 2021. "MATHEMATICAL MODELING FOR CARBON DIOXIDE LEVEL WITHIN CONFINED SPACES." International Mechanical Engineering Conference and Exposition 2021, American Society for Mechanical Engineers, IMECE2021-68452, November 2021, In Press.

Proceedings of ASME 2021 International Mechanical Engineering Congress and Exposition

(IMECE2021)

Volume 13

November 1-5, 2021
Virtual, Online

Conference Sponsor
American Society of
Mechanical Engineers

THE AMERICAN SOCIETY OF MECHANICAL ENGINEERS
Two Park Avenue * New York, N.Y. 10016

ISBN: 978-0-7918-8569-7

INTERNATIONAL MECHANICAL ENGINEERING CONGRESS & EXPOSITION

Dear Distinguished Attendees:

Welcome to the ASME 2021 International Mechanical Engineering Congress and Exposition (IMECE)! We are excited about this year, and continue to celebrate the **breadth**, **depth**, and **technical connections** that are the heart of a worthwhile conference experience. As you consider your schedule for this week, I personally invite you to benefit from each of these aspects of IMECE.

Breadth: 1350+ Technical papers and presentations over 14 technical tracks. At IMECE you can meet with experts from across the spectrum of mechanical engineering research and development. So, spend some time attending a few sessions outside of your technical area and see what you can take back to improve your own work.

Depth: Scientific expertise, not a trade show. From Nobel Laureates to one of the world's most cited researchers, the exceptional research depth at IMECE is nowhere so apparent as in the Congress-Wide Keynote Speakers and the Track Plenaries. For example:

- Dr. Shuji Nakamura, 2014 Nobel Laureate in Physics (Congress-Wide Keynote)
- Dr. Shery Welsh, Director of AFOSR with $500M in Basic Research (Aerospace Track Plenary)
- Dr. Nancy Sottos, Member of the NAE (Materials Track Plenary)
- Dr. Mehrdad Zangeneh, Founding Director of Advanced Design Technology, Ltd (Fluids Track Plenary)
- Dr. Yi Cui, one of the world's most cited scientists (Materials Track Plenary)

And these are just a few of the amazing speakers that will be available to you! Go to (https://event.asme.org/IMECE/Keynote-Speakers) and (https://event.asme.org/IMECE/Program/Track-Plenary) for the full list.

Technical Connections: 2,000+ attendees. The primary benefit of a conference is in meeting and interacting with fellow technical experts. As worldwide health conditions have forced us to remain virtual for a second year, we have implemented several new approaches to enable those interactions, and I invite you to fully participate. Our technical sessions have increased time scheduled for introductions and conversation before, during, and after the technical presentations (pre-recorded with live Q&A). And we have introduced a new series of special technical panels and roundtables designed to be technically focused informal gatherings. Topics for these 30–60-minute sessions range from "Nuclear Power in Space Applications: Promise, Practice, and Challenges" to "New Trends in Lung Therapies" to "Why Thermal Properties Still Matter", to "Advanced Manufacturing Education", "Beyond GPS: Advancing MEMS/NEMS Sensors for Inertial Navigation Only" and many more. The full list of Roundtables and Special Panels are on the congress website. Of course, nothing happens until you push the button. So, please join us! Whether in a technical session or special technical event, Turn on your camera, make a comment, ask a question, share an opinion, and build those connections!

Finally, on behalf of the IMECE Congress Steering Committee, I express my sincere thanks to and recognition of the hundreds of volunteers and the ASME staff that have dedicated time and effort to strengthening the fields of Mechanical Engineering R&D through organizing and leading sessions, topics, and tracks at this year's IMECE. It is never convenient to serve, and we have all continued to face frustrations of schedule, deadlines, conference websites, and more. Thank

you for your service. Your efforts have resulted in a strong congress that will continue to drive research forward both now and in the next generation. Thank you.

Sincerely,

Marriner H. Merrill, PhD
IMECE 2021 Technical Program Chair
Materials Science and Technology Division, US Naval Research Laboratory

STEERING COMMITTEE

Marriner Merrill
Technical Program Chair
U. S. Naval Research Laboratory

Dumitru (Micky) Caruntu
Technical Program Vice Chair
University of Texas – Rio Grande Valley

Chris Depcik
General Conference Chair
University of Kansas

Alberto Cuitino
Steering Committee Vice Chair
Rutgers – The State University of New Jersey

Olesya I. Zhupanska
Steering Committee Chair
University of Arizona

Stephen D. Tse
Steering Committee Senate Chair
Rutgers – The State University of New Jersey

Rama Koganti
Steering Committee Senate Member
University of Texas Southwestern Medical Center

Assimina Pelegri
Steering Committee Senate Member
Rutgers – The State University of New Jersey

George Kardomateas
Steering Committee Senate Member
Georgia Institute of Technology

Aaron Knobloch
Steering Committee Senate Member
GE Research

Albert Ratner
Member At Large
University of Iowa

Wenbin Yu
Member at Large
Purdue University

CONFERENCE ORGANIZERS

Acoustics, Vibration, and Phononics
Chair: Yongfeng Xu, *University of Cincinnati*
Co-Chairs:
Guoliang Huang, *University of Missouri*
Mostafa Nouh, *University at Buffalo*

Advanced Manufacturing
Chair: Chetan Nikhare, *Pennsylvania State University, Behrend*
Co-Chairs:
Muhammad Jahan, *Miami University*
Scott Thompson, *Kansas State University*
Yifei Jin, *University of Nevada, Reno*

Advanced Materials: Design, Processing, Characterization and Applications Chair: Hareesh Tippur, *Auburn University*
Co-Chair: Caglar Oskay, *Vanderbilt University*

Advances in Aerospace Technology
Chair: Erkan Oterkus, *University of Strathclyde*
Co-Chairs:
Pavana Prabhakar, *University of Wisconsin-Madison*
Uttam Chakravarty, *University of New Orleans*

Biomedical and Biotechnology Engineering
Chair: Linxia Gu, *Florida Institute of Technology*
Co-Chairs:
Ahmed Al-Jumaily, *Auckland University of Technology*
Martin Tanaka, *Western Carolina University*
Reuben Kraft, *Pennsylvania State University*

Design, Systems, and Complexity
Chair: Miri Weiss-Cohen, *Braude College of Engineering*
Co-Chairs:
Daniele Regazzoni, *University of Bergamo*
Marco Rossoni, *Politecnico di Milano*

Dynamics, Vibration, and Control
Chair: Micky Caruntu, *University of Texas-Rio Grande Valley*
Co-Chairs:
Eleonora Tubaldi, *University of Maryland*
Marco Amabili, *McGill University*

Energy
Chair: Hohyun Lee, *Santa Clara University*
Co-Chairs:
Michael Nistas, *National Technical University of Athens*
Reza Lakeh, *California State Polytechnic University, Pomona*
Soumik Banerjee, *Washington State University*

Engineering Education
Chair: Subha Kumpaty, *Milwaukee School of Engineering*
Co-Chairs:
Anabela Alves, *University of Minho*
Salim Azzouz, *Midwestern State University*

Fluids Engineering
Chair: Philipp Epple, *Coburg University of Applied Sciences*
Co-Chair: Kamran Siddiqui, *Western University*

Heat Transfer and Thermal Engineering
Chair: Ravi Annapragada, *Carrier Corporation*
Co-Chairs:
Alex Rattner, *Pennsylvania State University*
Kevin Dowding, *Sandia National Laboratory*

Mechanics of Solids, Structures, and Fluids
Chair: Marco Amabili, *McGill University*
Co-Chair: Celia Reina, *University of Pennsylvania*

Micro- and Nano-Systems Engineering and Packaging
Chair: Namwon Kim, *Texas State University*
Co-Chair: Gregory Hader, *Stevens Institute of Technology*

Safety Engineering, Risk and Reliability Analysis Chair:
Andrey Morozov, *University of Stuttgart*
Co-Chairs:
Alba Sofi, *University Mediterranea of Reggio Calabria*
Bill Munsell, *Munsell Consulting Services*
Ernie Kee, *University of Illinois Urbana-Champaign* Jennifer
S. Cooper, *Boeing*
John Wiechel, *SEA, Ltd.*
Mihai Diaconeasa, *North Carolina State University*
Zahra Mohaghegh, *University of Illinois Urbana-Champaign*

ASME Undergraduate Expo
Chair: Eleonora Tubaldi, *University of Maryland*

NSF
Chair: Siddiq Qidwai, *National Science Foundation*
Co-Chair: Marriner Merrill, *U. S. Naval Research Laboratory*

Research Posters
Chair: Omid Askari, *West Virginia University*
Co-Chairs:
Al Ratner, *University of Iowa*
Dorrin Jarrahbashi, *Texas A&M University*

REVIEWERS

Armin Abbasalinejad
Behrokh Abbasnejad
Moustafa Abdelhamid
Peter Abdo
Hasanain Abdulhadi
Arif Abdullah
Olayinka Abegunde
Kingsley Abhulimen
Omar Aboul-Enein
Mohammad Abshirini
Seena Abu
Zuruzi Abu Samah
Ma'moun Abu-Ayyad
Mohammed Abushamleh
Oyetunde Adeaga
Victor Adegboye
Solomon Adera
Adedotun Adetunla
Pashupati Adhikari
Ashfaq Adnan
Hassan Agalit
Michael Agarana
Ankush Aggarwal
Francesco Aggogeri
Vivek Agnihotri
Vipin Agrawal
Ebenezer Ahiati
Furqan Ahmad
Narendra Akhadkar
Bakytzhan Akhmetov
Murat Aksu
Hani Al Hazmi
Abdullah F. Alajmi
Fahd Alam
Mohammad Didarul Alam
Sheymaa Alazzawi
Muhamed Albadawi
Tyler Albright
Saleh Alhumaid
Ammar Ali
Abdulaziz Alkandari
Rami Alkhatib
Seyed Allameh
Brendon C. Allen
Mohammed Al-Mudhafar
Moza Alnaimi
Gioacchino Alotta
Saif Alrafeek
Mohammad Al-Rawi
Saja Al-Rifai
Saad Alshahrani
Ahmad Alshorman
Ahmed Alshwairekh
Anabela Alves
Sachin Alya
Marco Amabili
Rohan Amare
Catherine Ambrose
Ali Ameri
Alberto Amerini
Saeb AmirAhmadi Chomachar
Alireza Amirkhizi
Feruza Amirkulova
Luling An
Nadish Anand
Nishita Anandan
Kevin Anderson
Mohanish Andurkar
M. Anthony Xavior
Enrico Antonini
Noble Anumbe
China Rama Lakshman Anumolu
Eyyup Aras
Egemen Aras
Emanuele Vincenzo Arcieri
Tariq Arif
Aaron Armstrong
Alberto Arroyo
Muzammil Arshad
Muhammad Arslan
Rmanathan Arunachalam
Utsav Raj Aryal
Asaed Asaed
Rasoul Askari
Omid Askari
Mohamad Aslani
Md Saifuddin Ahmed Atique
Mystica Augustine Michael Duke
Stefan aus der Wiesche
Vikrant Aute
Kleio Avrithi
Mohsen Ayoobi
Saeed Azad
Martin Azese
Saad Aziz
Yousof Azizi
Salim Azzouz
Gnanavel B.K.
Alireza Babaei
Ridha Baccouche
Daniel Bacellar
Mehar Bade
Amit Bagchi
Johnny Bahri
Xin Bai
Christopher Bailey
Emerson Baker
Amirhamed Bakhtiarydavijani
Sayavur Bakhtiyarov
Ashok Bakshi
Alla V. Balueva
Arkasama Bandyopadhyay
Deb Banerjee
Portia Banerjee
Anjishnu Banerjee
Arnab Banerjee
Richa Bansal
Hua Bao
Corina Barbalata
Gustavo Barbosa

Erik Bardy
Brett Barker
Deibys Barreto
Mike Barringer
Gaurav Bartarya
Akinsanya Damilare Baruwa
J. Sadhik Basha
Muhammad Anser Bashir
Mary Bastawrous
Anirban Basudhar
Riccardo Becchi
Andrew Bellocchio
Roberto Belotti
Alberto Benato
Mohammed El Khalil Bendadi
Ryan Berke
Michael Beyer
Kiran Bhaganagar
Anantha Padmanabhan Bhagavatheeswaran
Pranav Bhounsule
Luigi Biagiotti
Linkan Bian
Cosimo Bianchini
Michele Bici
Joseph Bickson
Kazi Md Masum Billah
Christopher Billings
Joseph Bishop
Sayan Biswas
Nolan Black
Joseph Blochberger
James Bluman
Saran Srikanth Bodda
Sandra K.S. Boetcher
Brian T. Bohan
Giacomo Bonaccorsi
Carlos Borras Pinilla
Andrea Botta
Sebastiaan Bottenheim
Nikolaos Bouklas
Charbel Bou-Mosleh
M'Hamed Boutaous
Andrew Bowman
Gulcharan Brainch
Michael Brambley
Ivan Breslavsky
Nathan Brinkman
Alexander Brown
Antonio Bula
Clayton P. Byers
Shengze Cai
Ercan Cakmak
Zhen Cao
Yihan Cao
Yue Cao
Roberto Capata
Martina Capone
Giovanni Carabin
Luca Carbonari
Van Carey
Gianluca Carraro
Dumitru Caruntu
Jennifer Case
Osvaldo Castro
Pietro Catalano
Paride Cavallone
Oana Cazacu
Emrah Celik
Cesar Celis
David Cereceda
Wadie Chalgham
Edwin Chan
Nitin Chandola
Yanni Chang
Fernando Charrua-Santos
Arka P. Chattopadhyay
Somnath Chattopadhyay
Sergei Chekurov
Shawn Chen
Jie Chen
Jianli Chen
Leitao Chen
Haodong Chen
Jinwei Chen
Yilun Chen
Shu Chen
Guang Chen
Zhiyi Chen
Qun Chen
YungChia Chen
J.S. Chen
Daniel Chen
Jiangtao Cheng
Meng-Sang Chew
John Chew
Sheng-Wei Chi
Eric Chia
Manohar Chidurala
Rahul Chikurde
Peter Childs
Geetha Chimata
Abhijeet Chodankar
Junseo Choi
Jae-Won Choi
Paolo Cicconi
Lee Clemon
Lorenzo Cocchi
Kristin Cody
David Cohen
John Collinger
Giorgio Colombo
Filippo Colombo Zefinetti
Jennifer Cooper
Casey Corrado
Sol-Carolina Costa
John Cotter
Bryce Cox
Daniel Cox
Nathan Crane
Ricardo Cuenca-Alvarez
Zheng Cui
Shuang Cui
Anthony D Angelo
Shweta Dabetwar
Huwei Dai
Zhaohe Dai
Manab Kumar Das
Himanshu Dave
Michael Davidson

Ethan Davis
Shuvodeep De
Robert Dean
Ibrahim Deiab
Phillip Deierling
Xin Deng
Shikai Deng
Onur Denizhan
Scott DePaula
Christopher Depcik
Ryan DeWall
Pankaj Dhaka
T.S. Dhanasekaran
Marco Di Bartolomeo
Davide Di Battista
Mihai A. Diaconeasa
Joao Dias
Gerardo Diaz
Jerrold Dietz
Sheng Ding
Siyi Ding
Sunil Dingare
Aniruddha Dive
Nicholas DiZinno
Xiangyang Dong
Janet Dong
De Dong
Pei Dong
Pengfei Dong
John S. Donnal
Sushil Doranga
Haley Doude
James Downs
Xianping Du
Zhidong Du
Shawn Duan
Christopher Dumm
Christopher Duron
Debarun Dutta
Sandip Dutta
Anjali Dwivedi
Shiyuan E.
Arjun Earthperson
Williams Ebhota
Paul Egan
Stephen Ekwaro-Osire
Francisco Elizalde Blancas
Raed El-Jawahri
Mohamed Elsayed
Mahmoud Elsharafi
William Emblom
Doctor Enivweru
Philipp Epple
Jayakiran Reddy Esanakula
Roja Esmaeeli
Mehdi Esmaeilpour
Kandula Eswara Sai Kumar
John Evans
Tagir Fabarisov
Danial Faghihi
Tanvir Faisal
Y. Fan
Yin Fan
Liwu Fan
Jun Fang
Xiaomin Fang
Saman Farhangdoust
Amirhossein Farvardin
Milad Farzad
Mahsa Farzaneh
Arianna Fatahi
Fabio Fatigati
Olawale Fatoba
Claudio Favi
Shaw Feng
Jinyang Feng
Naheed Ferdous
Fábio Fernandes
Svitlana Fialkova
Robin Fisher
David Flodman
C.S. Florio
Laurie Florio
Tyler Flynn
Victor Manuel Fontalvo Morales
Emine Foust
Claiton Franchi
Giulio Franchini
Michael Frazier
Emma Frosina
Gen Fu
Konda Reddy G.
Xiang Gao
Yuan Gao
Qian Gao
Pedro De Jesus García Zugasti
Zacharias Garza
Andrew Gaynor
Ozhan Gecgel
David Gee
Takele Gemeda
Joshua Gess
Levon Ghabuzyan
Amin Ghadami
Aref Ghaderi
Hamed Ghaffari
Fadi Ghaith
Mohsen Ghamari
Samad Gharehdaghi
Suhash Ghosh
Dipannita Ghosh
Anthony Giachin
Duncan William Gibbons
James Gibert
Antoni Gil Pujol
Axel Glahn
Emmanuel Glakpe
Aneesha Gogineni
Nathaniel Goldfarb
Yiska Goldfeld
Humberto Gomez Vega
Ugrasen Gonchikar
Stefano Gonella
Hernando Gonzalez
Arturo González
Germanico Gonzalez Badillo
Kalyan Goparaju

Yimy. Gordon
Recep M. Gorguluarslan
Ravi Gorthala
James Griffin
Tyler Grimm
Philipp Grimmeisen
Yaroslav Grosu
Chenchen Gu
Linxia Gu
Yuyang Gu
Shuitao Gu
Peng Guan
Guillermina Guerrero
David Guirguis
Rasim Guldiken
Amol Gulve
Yu Guo
Hong Guo
Zongqi Guo
Yang Guo
Zheng Guo
Tanuj Gupta
Anuj Gupta
Aniket Gupta
Sonam Gupta
Srinivasa Rao Gurrala
Sathish Kumar Gurupatham
Khan Habeeb Ur Rahman
Grzegorz Hader
Noah Hafner
Bhuiyan Shameem Mahmood Ebna Hai
Salim Haidar
Taher Hajilounezhad
Henry Haley
Peter Hamlington
Mostafa Hamza
Mohamed Hamza
Li-Hsin Han
Hai-Chao Han
Julie Hao
Matt Harrison
Mostafa Hassanalian
Pezhman Hassanpour
Grant Hawkes
Andrew Hayden
Jiaze He
Kai He
Rui He
Ge He
Nathaniel Heathman
Cole Hefner
Anwar Hegazy
James Heidmann
Michael Hennessey
Daniel Herber
Tomas Hermansson
Abel Hernandez-Guerrero
Blake Herren
Morteza Heydari
Juan Luis Higuera-Trujillo
Michael Hillman
Mohammad Hodaei
Wyatt Hodges
John Homer
Peyman Honarmandi
Senhao Hou
QiTao Hou
Jiacheng Hou
Linzao Hou
Larry Howlett
Quang-Cherng Hsu
Yuhang Hu
Ming Hu
Kui Hu
Weijian Hua
Cathy Huang
Guoliang Huang
Bradley Huddleston
Hugo Hultman
Gabriele Humbert
Matti Huotari
Mahmoud Hussein
Parsaoran Hutapea
Gisuk Hwang
Lee Hyun Jae
Matthew Iannacci
Stephen Idem
Patricia Iglesias Victoria
Zeki Ilhan
Danny Illera Perozo
Miho Ishii-Teshima
Saif Mohammad Ishraq Bari
Nazmul Islam
Mahmudul Islam
Didi Istardi
Teruaki Ito
Brian D. Iverson
Anthony Izaguirre
Nathan Jackson
Suchana Akter Jahan
M.P. Jahan
José Jimmy Jaime Rodríguez
Abhishek Jain
Ankur Jain
Divya Jaladi
Hadi Jalali
Tausif Jamal
Sagil James
Ricardo Jardim-Goncalves
Esam Jasim
Carolina Jauregui
Sanjib Jaypuria
Robabeh Jazaei
T.R. Jebieshia
Selvaraj Jegadheeswaran
Songbai Ji
Xiaoxu Ji
Weiqi Ji
Yikai Jia
Tao Jia
Xiaoning Jiang
Zhiyuan Jiang
Zhu Jiang
Xin Jin
Jianhang Jin
Yifei Jin
Xusheng Jing
Jeanne Joachim

Mathew John
Murray Johnston
Matthew Jones
Michael Jonson
Sung-hwan Joo
Kris Jorgensen
Hamed Kalami
Onur Can Kalay
Hisham Kamel
Nitin Kamitkar
Kiana Kamrani Fard
K Kanishk
Sathish Kannan
Daniel Kaplan
Anargyros A. Karakalas
Kostas Karazis
Fernando Karg Bulnes
Soroor Karimi
Amir Karimi
Shashank Karra
Bright Katey
Ernest Kee
Eugenia Kennedy
Fardin Khalili
Jobaidur Khan
Mohammad Khan
Sufia Khatoon
Ryan Khawarizmi
Lyes Khezzar
Namwon Kim
Hanseul Kim
Seunghee Kim
Byungki Kim
Jungho Kim
Dongsu Kim
Hyun Jin Kim
Dohwan Kim
Owen Kingstedt
Vidya Kishore
Janardhan Kodavasal
Pratik Koirala
Kranthi Kolli
Jason Kolodziej
Teja Konduri
Behrad Koohbor
Matthew Korey
Satyanarayana Kosaraju
Basavraj Kothavale
Nitin Ramesh Kotkunde
Reuben Kraft
James Kribs
Nitin Nagesh Kulkarni
Rajesh Kumar
Deepak Kumar
Anil Kumar
Subha Kumpaty
Robert Kunz
Jim Kuo
Harsha Kusnoorkar
Vladimir Kuts
Sang Muk Kwark
Reza Lakeh
Ritesh Lakhkar
Prasanth Anand Kumar Lam
Asheesh Lanba
Daniele Landi
Horst Lanzerath
Michael Lapera
Curt Laubscher
William Lawrimore
Xiaobin Le
Francesco Leali
Michael Leamy
E.J. LeBlanc
Elias Ledesma Orozco
Juhyeong Lee
Chang-Chun Lee
Ho-Hoon Lee
Moo-Yeon Lee
Hohyun Lee
Christopher Lee
Peter Lee
Kun-Lin Lee
Taehun Lee
Ming-Tsang Lee
Juyoung Leem
Victor Lefevre
Devanda Lek
Tommaso Lenzi
Yanfei Li
Yongqiang Li
Puxuan Li
Zhichao Li
Xianglin Li
Hua Li
Yaofa Li
Jinglun Li
Yanjun Li
Mingzhe Li
Zhimin Li
Zhiye Li
Zhenxing Li
Gang Li
Tianchu Li
Yumeng Li
Bo Li
Weitao Li
Chao Liang
Hong Liang
Xiong Liang
Theo Lim
Sheng-Min Doris Lin
Zhibin Lin
Jiazhen Ling
Noam Lior
Andrew Littlefield
Haowen Liu
Haidong Liu
Yao-Hsien Liu
Yucheng Liu
Ling Liu
Tao Liu
Xin Liu
Qingchang Liu
Yingtao Liu
Tangzhu Liu
Haijun Liu
Summer Locke
Robert L. Lowe
Saul Loza
Zexi Lu

Qi Lu
Qiyue Lu
Weiyi Lu
Dirk M. Luchtenburg
V.T. Lukong
Sergey Lupuleac
Jianfeng Ma
Zhen Ma
Yuliang Ma
Haibo Ma
David Mabelane
Brianna MacNider
Ebrahim Maghami
Ameneh Maghsoodi
Mohammad Maghsoudi-Ganjeh
Mahboobe Mahdavi
Mohammad Mahinfalah
Kashif Mahmood
Mohammadreza Mahmoudi
Pooya Mahmoudian
Mohammad Mahtabi
Varad Maitra
Dipanjan Majumdar
Yelaman Maksum
Sepehr Maktabi
Rahul Makwana
Subhasish Malik
Mahmood Mamivand
Dilip Mandal
Giovanni Manente
Randall Manteufel
Maurizio Manzo
Jessica Gissella Maradey Lazaro
Jared Marcel
Marco Marconi
Christopher Martin
Jose Israel Martinez Lopez
Roberto Martinez-Montejano
Jeremy Marvel
Matthew Maschmann
Kathryn H. Matlack
Kathryn Maupin
Lorenzo Mazzei
James McCusker
Kevin McMullen
Joshua Mctigue
Tanmoy Medhi
Arash Mehraban
Hil Meijer
Shabbir Memon
Julie Mendez
Gregory Meyer
Tianwei Miao
Siamak Mirfendereski
Kyran Mish
M.P. Mishra
Arpit Mishra
Samy Missoum
Sridhara Rao Mittapalli
Mohand Mohamed
Walid Mohamed
Hamid Mohammadi
Ram Mohan
Lokanath Mohanta
Lesego Mohlala
Vera Moiseytseva
Wael Mokhtar
A.K.M. Monayem H. Mazumder
Keegan Moore
Vito Moreno
Carlos Luis Moreno Negrin
Andrey Morozov
Mehdi Mortazavi
Ershad Mortazavian
Mojtaba Moshtaghzadeh
Fan Mu
Muhammed Muaz
Partha P. Mukherjee
Saptarshi Mukherjee
Subrata Mukherjee
Arun Muley
Rydge Mulford
Manuel Müller
Sungkwang Mun
Troy Munro
William Munsell
Joydeep Munshi
Giuseppe Muscolino
Satish Muthu
Mamoona Muzammil
Avitus Mwelinde
Aggrey Mwesigye
Mahdi Nabil
Rajesh Nagadolla
Moeto Nagai
Shailendra Naik
Kalyani Nair
Hamidreza Najafi
Ali Najafi
Ahmad Najafi
Ahad Nasab
Farshad Navah
Helena Navarro
Kashif Nawaz
Ivaylo Nedyalkov
Ezz El-Din Nehad Mostafa
George Nelson
Samuel C. Neu
Vinh Nguyen
Xinchen Ni
Chetan Nikhare
Pouriya Niknam
Joachim Nilsen Grimstad
Xin Ning
Michail Nitsas
Arman Nokhosteen
Mostafa Nouh
Margaret Nowicki
Saied Nusier
John Nuszkowski
Andrzej Nycz
Aronu Obinna
Gregory Odegard
Hannah O'Hern
Jeong Tae Ok
Andreas Olympios
Sameer Osman

Selda Oterkus
Saad Oudah
Sunday Olayinka Oyedepo
Hakan Ozaltun
Vijay Pachore
Darshan Pahinkar
Rishi Pahuja
Brian Painter
Rajendra Prasath Palanisamy
Kevin Pan
Heng Pan
Kapil Panchal
Hitesh Panchal
Priyanka Pandit
Junru Pang
Amrinder Singh Pannu
Lalit Pant
Alessandra Papetti
John Pappas
Anatoly Parahovnik
P. Parameswaran
Mihir Parekh
Keunhan Park
Chanwoo Park
Hoonmin Park
Omkar Parkar
Maximilian Passmann
Michael Pate
Darshil Patel
Dhiren Patel
Kavi Patel
Sandeep Patil
Brandon Patterson
Uma Maheshwera Reddy Paturi
Brent Paul
Titan Paul
Vivek Pawar
Srinivasa Rao Pedapati
Reza Pejman
Assimina Pelegri
Vladimir Pena
Fang Yu Peng
Edwin Peraza Hernandez
Salman Pervaiz
Mohnish Peswani
Marco Petrolo
Michael Pettes
Tomasz Piatkowski
Roy Pillers
Fabio Pini
Pius Pius
Matthew Plutt
Pranaya Pokharel
Burak Polat
Wilma Polini
Bibek Poudel
Ricardo Poveda
Vinit Prabhu
Jose I. Prado
Raghu V. Prakash
Anchasa Pramuanjaroenkij
Hariyo Priambudi Setyo Pratomo
William Prescott
Cristina Prieto
Ernesto Primera
Prashant Chandra Pujari
Marco Puliti
Mohammad Khairul Habib Pulok
Tuomas Puttonen
Dong Qian
Xin Qian
Dongsheng Qiao
Guangzhao Qin Qin
D. Dane Quinn
Tãµnis Raamets
Hassan Raheem
Peyman Rahimi Borujerdi
S.M. Mahbobur Rahman
Mohammad Rizwen Ur Rahman
M. Shafiqur Rahman
Mahabubur Rahman
Manjunath C. Rajagopal
Anurag Rajagopal
Vomsheendhur Raju
Chandra Sekhar Rakurty
Manoj Ram
Karthikeyan Ramanujam
Vaishak Ramesh Sagar
Angel D. Ramirez
Maria Ramos Gonzalez
Mohammadreza Ramzanpour
Zhongnan Ran
G.M. Rahid Uz Zaman Rana
Nithin Rangasamy
Rakesh Ranjan
Jing Rao
Fayaz Rasheed
Anton Rassõlkin
Shubham Rath
Albert Ratner
Alexander Rattner
Marisha Rawlins
Bahni Ray
Sergio Rech
Daniele Regazzoni
Sambad Regmi
Giulio Reina
Mitchell Rencheck
Ramjee Repaka
Benoit Revil-Baudard
Marcos Reyes-Martinez
Abolfazl Rezaei Aderiani
Elnaz Rezaian
Dong-Ho Rhee
Jovica Riznic
Caterina Rizzi
Nicholas Roberts
Franklin Robinson
Frederico Rodrigues
Marcelo Rodrigues Fernandes
Hee Seok Roh
Ajith Krishnan Rohini
Freddy Jesus Rojas Chavez

David Romero
Cameron Rose
Marco Rossoni
Michael Roth
S. Rouhi
Shrabanti Roy
Arnab Roy
Bikram Roy Chowdhury
Xiulin Ruan
Christopher Rudolf
Eric Ruggiero
David Ruiz
Sangjin Ryu
Lakshmi S.
Ahmed S. Saad
Parisa Saboori
Ibrahim Sabry
Ahsana Sadaf
Roham Sadeghi Tabar
S. Sadeqi
Babak Safaei
Amrit Sagar
Pankaj Saha
Sujoy Saha
Sudipta Saha
Ujjwal K. Saha
Probir Saha
Lokesh Saharan
Iskender Sahin
Bijoyraj Sahu
Muhammed Saif
Anil Saigal
Hani Sait
Roozbeh (Ross) Salary
Khaled Sallam
Santhakumar Sampath
Mauricio Sanchez
Juan Sandoval
Sridhar Santhanam
Kaushik Sarkar
Pratik Sarker
Jyotirmoy Sarma
Robert Saunders
Toshiyuki Sawa
Lorenzo Scalera
Olivia Scheibel
Frank Schieck
Matthew Schifano
Gillian Schiffer
Bryan Schmidt
Anne Schmitz
Adriano Sciacovelli
Majura Selekwa
Rajiv Selvam
Soroush Sepahyar
Michael Sevier
Eduard Ševtšenko
Arash Shadlaghani
Harshal Y. Shahare
Ashu Sharma
Rajeev Sharma
Preet Sharma
Mostafa Shazly
Zhengjing Shen
He Shen
S.A. Sherif
Shuquan Shi
Yuan Shi
Yunye Shi
Jingjing Shi
Tom Shih
Sidney Bruce Shiki
Saeed Shiri
Md. Imrul Reza Shishir
Olalekan O. Shobayo
Jamileh Shojaeiarani
Wan Shou
XueDao Shu
Ashwin Siddarth
Mathieu-Antoine Sierro
João Silva
Abhishek Kumar Singh
Nityanand Sinha
Ashish Sinha
Ahmad Sleiti
Dean Snelling
Rikard Söderberg
Alba Sofi
Ratnak Sok
Abhijit Som
Wangbing Song
In-Hyouk Song
Jinwoo Song
Guangchao Song
Li Song
Zhengyi Song
Xiaolei Song
Hoanan Song
Yooseob Song
Mehmet Sozen
McKay Sperry
Vinod Srinivasan
Rajeshwar Sripada
Ankit Srivastava
Terrin Stachiw
John Steimke
Vesselin Stoilov
Gabriel Streitmatter
Samuel Subia
Harish Subramanyan
Prathik Jain Sudhir
Taylor Suess
C. Steve Suh
Yunyun Sun
Lei Sun
Haining Sun
Wangping Sun
Shung-hsing Sung
Vyshak Sureshkumar
Ehsan Taati
Alireza Tabarraei
Alex Tacescu
Luca Tagliafico
Hossein Taheri
Abdul Raouf Tajik
Siddharth Talapatra
Lorenzo Talluri
Ilie Talpasanu
Atsutaka Tamura
Kwek-Tze Tan
Hua Tan
X. Gary Tan

Martin Tanaka
Hui Tang
Jinsong Tang
Yash Tank
Khalid Tantawi
Buddi Tanya
Akin Tatoglu
Dorothy Taylor
Mehran Tehrani
Khashayar Teimoori
Ayse Tekes
Halil Tekinalp
John Tencer
Zhiqiang Teng
Alp Tezbasharan
Mishal Thapa
Scott Thompson
Zhenhua Tian
Ang Tian
Saeed Tiari
Juan Tibaquira
Ankit Tiwari
Beth Todd
Ravi Pratap Singh Tomar
Mukul Tomar
Robert Tomko
Casey Troxler
Eleonora Tubaldi
Göker Türkakar
Pawan Tyagi
James V. Cox
Luca Valdarno
R. Michael Van Auken
Kenneth Van Treuren
K. Philip Varghese
Thomas Vasko
Kostiantyn Vasylevskyi
Andrea Vecchi
Arun Veeramany
Ruben Venegas
Holalu Venkatdas Ravindra
Chadalavada Venkateswara Babu
Ankit Verma
Riccardo Vescovini
Carlos Ramón Vidal Tovar
Jose L. Viesca
Umberto Villa
Vimal Viswanathan
Andrea Vitali
Diego Vittorini
Kelen Cristiane Teixeira Vivaldini
Gabriele Volpato
Tung Vuong
Anand Vyas
Adam Wachtor
Ian Walker
Graham Walker
D.K. Walters
Xingyu Wang
Michael Cai Wang
Xinwei Wang
Yeqing Wang
Qiming Wang
Jingyu Wang
Wei Wang
Junzhen Wang
Curtis Wang
Zhenyu Wang
Yan Wang
Peng Wang
Jianhua Wang
Wenxi Wang
Shiyan Wang
Xueju (Sophie) Wang
Kristina Warmefjord
Ronald Warzoha
Dane Wedgeworth
Justin Weinmeister
Miri Weiss Cohen
Yi Wen
John Wiechel
Enakshi Wikramanayake
Sara Wilson
Stephanie Wimmer
Keo-Yuan Wu
Zhijun Wu
Chenglin Wu
Mingtao Wu
C.T. Wu
Wenxuan Xia
Yingxiang Xia
Xiao Xiangyu
Xinyi Xiao
Angran Xiao
Gongnan Xie
Zhuowen Xie
Siyuan Xing
Ruitong Xiong
Luoyu Xu
Jun Xu
Yongfeng Xu
Yeyin Xu
Minghan Xu
Tongge Xu
Baoxing Xu
Wei Xue
Reza Yaghmaie
Sami Yamanidouzisorkhabi
Karen Chang Yan
Ling Yan
Lincan Yan
Chen Yan
Zhuo Yang
Chun-Lin Yang
Yichao Yang
Mengqiao Yang
Bingen (Ben) Yang
Haoqing Yang
Song Yang
Shujie Yang
Xiaolong Yang
Weizhu Yang
Zhonghua Yang
Yifei Yao
Wei Yao
Timothy Yap
Taiho Yeom
Ravinder Yerram

Sumith Yesudasan Daisy
Steven Yip Fun Yeung
Ho Yeung
Guilian Yi
Salih Yildiz
Sha Yin
Akio Yonezu
William Young
Kianoosh Yousefi
Cunjiang Yu
Kai Yu
Hong Yu
Zexing Yu
Pengyu Yuan
Chunhao Yuan
Sichen Yuan
Zhangxian Yuan
Andrei Zagrai
Md. Zahid Hasan
Guiyan Zang
Jian Zeng
Chi Zhan
Lufan Zhang
Ning Zhang
Wei Zhang
Lin Zhang
Kaihao Zhang
Yanmei Zhang
Wen Zhang
Zhou Zhang
Zilong Zhang
Jianan Zhang
Xiaoliang Zhang
Jing Zhang
Chao Zhang
Zhifeng Zhang
Xiaoyu Zhang
Liang Zhang
Chen Zhang
Yue Zhang
Jian Zhang
Nathan Zhang
He Zhang
Min Zhang
Yongqing Zhang
Mingshao Zhang
Peiran Zhang
Peter Zhang
Qinqiang Zhang
Haipeng Zhang
Dianyun Zhang
Yating Zhang
Xian Zhang
Man Zhao
Huijuan Zhao
Shijia Zhao
Kai Zhao
Changlong Zheng
Cao Zhi
Allan Zhong
Hong Zhou
Yanguang Zhou
Min Zhou
Zenghao Zhu
Linda Zhu
Linqi Zhuang
Wei Zhuang
Metodi Zlatinov
Hamidreza Zobeiri
An Zou
Ahmad Zueter

CONTENTS

Proceedings of ASME 2021 International Mechanical Engineering Congress and Exposition Volume 13

Machine Learning for Safety, Reliability, and Maintenance

Models and Methods for Probabilistic Risk Analysis

Probabilistic Risk Assessment of Protective Systems

Reliability and Risk in Energy Systems

Reliability and Safety in Industrial Automation Systems

Reliability and Safety in Transportation Systems

Reliability and Safety of Deep Learning-Based Components

Student Safety Innovation Challenge

Heat Transfer and Thermal Engineering

Mechanics of Solids, Structures, and Fluids

Safety Engineering, Risk, and Reliability Analysis